Passivity Enhancement of Voltage-Controlled Inverters in Grid-Connected Microgrids Considering Negative Aspects of Control Delay and Grid Impedance Variations

Akhavan, Ali; Golestan, Saeed; Vasquez, Juan C.; Guerrero, Josep M.

Published in:
IEEE Journal of Emerging and Selected Topics in Power Electronics

DOI (link to publication from Publisher):
10.1109/JESTPE.2021.3065671

Publication date:
2021

Document Version
Accepted author manuscript, peer reviewed version

Passivity Enhancement of Voltage-Controlled Inverters in Grid-Connected Microgrids Considering Negative Aspects of Control Delay and Grid Impedance Variations

Ali Akhavan, *Member, IEEE*, Saeed Golestan, *Senior Member, IEEE*, Juan C. Vasquez, *Senior Member, IEEE*, and Josep M. Guerrero, *Fellow, IEEE*

***Abstract*—With growing environmental concerns, the installation of distributed generation systems forming microgrids in power systems has received much attention recently. This panacea, however, has always some challenges with itself. The delay in digital control systems, grid impedance variations in weak grids, and the interaction between paralleled converters in a microgrid, which can threaten the expectable operation of microgrids, are notable examples. Thus, this paper formulates these challenges in microgrids and then addresses them so that guarantees the stable operation of the microgrid. To this end, this paper first offers a delay compensation method, and elaborates it so that the control system achieves a high robustness against grid impedance variations. Then, a feedforward loop is introduced to the control system that makes the system immune against the interaction of inverters in microgrids. Using these methods, the system can survive irrespective of the above-mentioned non-ideal conditions. The grid-forming control approach is selected as the operation mode of the microgrid in this paper, since it could be used for both grid-connected and islanded scenarios. The experimental results of a laboratory prototype show the correctness of the theoretical conclusions and confirm the efficiency of the suggested technique.**

***Index Terms*— Control delay, interaction, grid-forming inverters, microgrids, stability.**

I. Introduction

Grid-interactive power converters play a key role in interfacing renewable energy systems to the power grid. Therefore, their control and stability is an issue of paramount importance [1], [2]. Often, a grid-following control mode is adopted for the control of grid-connected inverters that means they are regulated to follow a reference current [3]–[5]. The stability assessment of grid-connected inverters in this operation mode has been well discussed in the literature [6]–[11]. The grid-forming operation mode is an alternative option for the control of grid-connected inverters [12], [13]. Such an operation mode is often adopted under weak grids to support the power grid in stabilizing the voltage/frequency or when an intentional/unintentional islanding happens. On the other hand, this control mode could be adopted for a smooth transition between grid-tied and islanding mode. Unfortunately, the research works on the stability assessment of the grid-interactive inverters in this operation model are limited. Therefore, the stability of voltage-controlled inverters should be investigated further in different case studies and by considering non-idealities, such as computational and PWM delay, grid impedance variations as well as coupling effect among parallel inverters.

The voltage-controlled inverters with an *LC* or *LCL* filter have been extensively used for distributed generation systems [14], uninterruptible power supplies [15], and grid emulators [16], among other applications. To ensure a satisfactory operation, normally a double-loop control method comprised of an inner loop for controlling the current, and an outer loop for controlling the voltage is used [17]. In this scheme, the inner loop could be modeled as a virtual impedance that is in series with the inverter-side inductor. Thus, it has an inherent active damping for the mitigation of filter resonance. The virtual impedance is affected by the delay in digitally-controlled systems and might cause instability issues.

The delay introduces some problems for control of the inverter such as negative virtual impedance and signal aliasing [18]. The virtual impedance behaves as a negative resistance at frequencies higher than $f_s/6$, where f_s is the sampling frequency. Therefore, the loop gain will have right-half-plane (RHP) poles in a case that the resonance frequency of the filter capacitor and inverter-side inductor is higher than the critical frequency $f_{cr} = f_s/6$. Therefore, the system is prone to a non-minimum phase behavior because of RHP poles, which might make the system unstable [19].

Extensive researches have been done to amend the adverse effect of the delay on the control system. A reciprocal of a notch filter and a high-pass filter are proposed in [20] and [21], respectively, to reduce the delay's negative effect. In [22], sampling instant is shifted to amend the delay effect. However, the implementation of this method is prone to switching noise and signal aliasing. Li *et al.* [23] proposed a repetitive-based control system for the delay compensation to expand f_{cr}. However, this method puts the system at the risk of noise amplification at the Nyquist frequency because of infinite gain at this frequency. An observer-based method is proposed in [24] to predict the current and amend the delay

This work was supported by VILLUM FONDEN under the VILLUM Investigator Grant (no. 25920): Center for Research on Microgrids (CROM).

This article has been accepted for publication in a future issue of this journal, but has not been fully edited. Content may change prior to final publication. Citation information: DOI 10.1109/JESTPE.2021.3065671, IEEE Journal of Emerging and Selected Topics in Power Electronics

effect. However, this method might suffer from parameters mismatch, since it is sensitive to uncertainties and parameter variations. Pan *et al.* [25] proposed an optimized capacitor current feedback-based active damping for resonance mitigation in a digitally-controlled system.

Although all the above-mentioned studies and many others have been carried out on the delay compensation, few of them have focused on the concept of passivity. The passivity, in simple words, means that the converter output impedance has a positive real part. In this way, irrespective of the grid impedance value and its possible variations, the converter can preserve its stability [26].

Additionally, another challenge that comes to mind is the coupling effect of parallel converters in a microgrid, especially when a number of parallel converters are connected to a point of common coupling (PCC). In this case, because of the coupling effect among parallel units, the equivalent grid impedance that each inverter sees in its output will be different from the actual grid impedance, which may cause instability issues [27]–[29]. Notice that if the inductive grid impedance intersects with inverter output impedance in its capacitive range, where the real part of the inverter output impedance is negative, it puts the system at the risk of instability [30]. This situation is a probable scenario in weak grids where the grid impedance varies in a wide range or in multi-parallel systems, where connecting or disconnecting an inverter affects the grid impedance seen by other inverters.

The passivity concept provides an intuitive approach to investigate the harmonic stability problem and minimize the frequency range where the converter has a negative resistance behavior [30]. In fact, the goal of passivity-based stability is to provide a condition for all connected sub-systems to have a passive and stable behavior in a wide range of frequency. In this condition, the system keeps its stability irrespective of the grid impedance variations and the number of parallel inverters, as each element is solely passive.

Passivity-based stability has been increasingly studied in the literature [29]–[34]. Yoon *et al.* [29] have shown the interaction of non-passive inverters in a microgrid with varying grid impedance. The inverter output impedance is decomposed into a passive and an active impedance in [31], where the passive impedance depends on the *LCL* filter, and on the other hand, the current controller and the time delay affect on the active impedance. The passivity of a single-loop voltage-controlled inverter is addressed in [32]. In [33], a series *LC*-filtered active damper is proposed to mitigate the resonance. It could be used for passivity enhancement but adding an extra converter increases the cost and complicates the control system. A similar idea is proposed in [34], in which the grid impedance effect is mitigated using an active filter. A modified controller is proposed in [35] to amend the phase of inverter output impedance in a current-controlled grid-connected inverter.

The majority of the above passivity-based studies have been conducted on the current-controlled systems, and very limited works have been carried out on the voltage-controlled systems. Bridging this research gap is the main aim of this paper. To this end, this paper presents an in-depth stability analysis of a dual-loop voltage-controlled inverter. The effect of delay in digitally-controlled systems on the stability of the system is first analyzed, comprehensively. The negative effect of delay is compensated by introducing an adequate positive phase to the system through a lead-lag filter. Thus, the critical frequency is expanded to frequencies higher than $f_s/6$. This method could be useful for systems in which the sampling frequency is relatively low or the resonance frequency is higher than $f_s/6$. Also, a control system with a wide bandwidth is designed to ensure a satisfactory operation. A step-by-step controller design is presented for each part. Then, an output current feedforward method is proposed, which guarantees the stability of the system irrespective of the grid impedance variations and the coupling effect among the parallel inverters. By using the proposed methods, it will be shown that the inverter output impedance keeps its passivity up to the Nyquist frequency. The proposed methods in this paper can be used in the case of control voltage in islanded microgrids, as well.

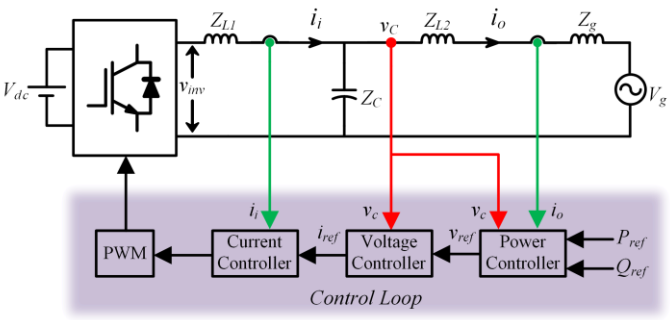

Fig. 1. Voltage control structure of a grid-connected inverter.

The rest of this paper is organized as follows. In Section II, a short description of the system, as well as delay effect, are presented to formulate the problem. In Section III, a delay compensation method is presented to improve the system robustness. In Section IV, the stability of the system based on the passivity is discussed and an output current feedforward method is proposed to achieve a stable condition for the inverter. In Section V, the proposed methods are validated through comprehensive analysis and experimental results. Finally, the paper is concluded in Section VI.

II. System Modeling and Problem Definition

The voltage control structure of a grid-connected inverter is shown in Fig. 1. In this figure, Z_{L1} and Z_{L2}, are the impedance of the inverter-side and grid-side inductors, respectively. Z_C denotes the capacitor impedance, and Z_g is the grid impedance.

$$Z_{L1} = L_1 s,\ Z_{L2} = L_2 s,\ Z_C = \frac{1}{Cs},\ Z_g = L_g s \tag{1}$$

As the resistive components offer some damping and help stabilize the system, they are neglected here to take into account the worst-case scenario.

As shown in Fig. 1, the inverter output is regulated using a dual-loop control structure, where the outer loop controls the capacitor voltage and the inner loop regulates the inverter side

This article has been accepted for publication in a future issue of this journal, but has not been fully edited. Content may change prior to final publication. Citation information: DOI 10.1109/JESTPE.2021.3065671, IEEE Journal of Emerging and Selected Topics in Power Electronics

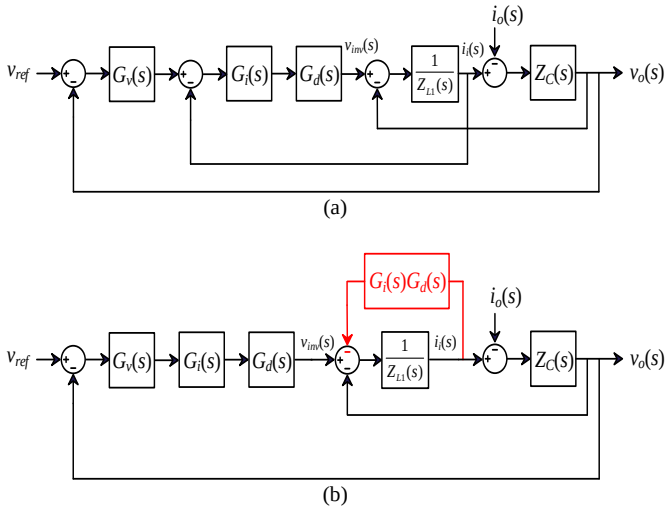

Fig. 2. The control scheme of the traditional voltage-controlled inverter. (a) The traditional double-loop voltage control. (b) Mathematically-equivalent single-loop representation of the double-loop voltage control.

current. The reference voltage is generated using a power controller, which has a much lower bandwidth compared to the voltage and current control loops. Therefore, without significantly affecting the accuracy, its dynamics can be neglected in the stability assessment of the voltage and current control loops, which is the focus of this paper. Refer to [36] for more details about the dynamics of the power controller and its design procedure.

The study in this paper is carried out in the $\alpha\beta$ frame, which is realized by applying the Clarke transformation to the three-phase voltage and current signals. Considering that the system is supposed to be symmetrical, alpha and beta axes of voltage and current control loops are identical and therefore, could be treated like a single-phase system.

The control block diagram of the traditional dual-loop voltage-controlled grid-connected inverter is presented in the $\alpha\beta$ frame in Fig. 2(a), in which $G_v(s)$ and $G_i(s)$ are the voltage and current controllers, respectively. $G_d(s)$ models the computational and PWM delay, is equal to [20]

$$G_d(s) = e^{-1.5T_s s} \tag{2}$$

where T_s denotes the sampling period.

Regarding Fig. 2(a), the first thing that comes to mind is that the grid-side inductor (L_2) can be considered as a part of the grid impedance and it does not affect the system dynamics. The effect of the grid-side inductor on the system stability will be investigated in Sections IV and V.

In the dual-loop control system, a proportional regulator is normally used as the inner current loop controller [32]. Therefore, $G_i(s) = k_{pi}$ is considered in this paper. By applying the block diagram algebra to Fig. 2(a), it could be represented, as shown in Fig. 2(b). This representation shows that the inner loop could be modeled as a virtual impedance $Z_v(s)$ in series with the inverter-side inductor. $Z_v(s)$ is presented as

$$Z_v(s) = G_i(s)e^{-1.5T_s s} = k_{pi}e^{-1.5T_s s}. \tag{3}$$

Fig. 3 shows the equivalent circuit of a dual-loop voltage-controlled grid-connected inverter. Thus, the dual-loop control

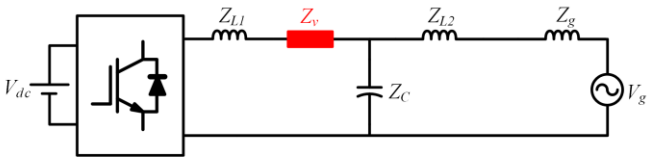

Fig. 3. Equivalent circuit of a dual-loop voltage-controlled grid-connected inverter.

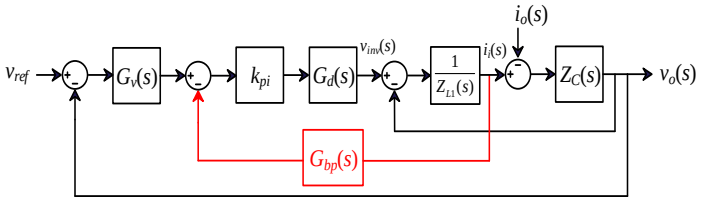

Fig. 4. The proposed control system for expanding f_{cr}.

system has an inherent active damping which mitigates the resonance of the filter and therefore, improves the system stability.

By applying the Euler's formula and considering $G_i(s)$ as a proportional controller, $Z_v(s)$ can be represented as follows:

$$Z_v(j\omega) = k_{pi}[\cos(1.5\omega T_s) - j\sin(1.5\omega T_s)]. \tag{4}$$

From (4), it could be easily found that the real part of the virtual impedance is positive for $0 < f_{cr} < f_s/6$ and negative for $f_s/6 < f_{cr} < f_s/2$ [37]. Therefore, the system loop gain will have RHP poles when the resonance frequency of the filter capacitor (C) and inverter-side inductor (L_1) is higher than $f_s/6$, which in turn, might make the control system unstable [19]. In this condition, the virtual impedance not only does not improve the system stability, but also puts the system at the instability risk.

It should be noted that if the delay is ignored, the virtual impedance turns to a resistor. However, the negative phase that comes from the delay changes the ideal condition. Therefore, expanding the critical frequency (f_{cr}) is the first step for the stable operation of the inverter.

III. Delay Compensation

In this section, a method using a lead-lag filter for delay compensation and expanding the critical frequency is presented, and its tuning aspects are discussed.

A. Lead-Lag Filter-Based Delay Compensation

In order to expand the critical frequency and, therefore, enhance the stability of the active damping loop (inner loop) against the resonance frequency, the critical frequency should be increased. To this end, the phase lag introduced by the delay must be amended. Here, using a lead-lag filter is suggested for this purpose. The lead-lag filter is inserted along the inner feedback path as shown in Fig. 4. Its transfer function is presented as

$$G_{bp}(s) = k_{bp}\frac{s+\omega_\alpha}{s+\omega_\beta} \tag{5}$$

where ω_α and ω_β are its corner frequencies and k_{bp} is its gain.

This article has been accepted for publication in a future issue of this journal, but has not been fully edited. Content may change prior to final publication. Citation information: DOI 10.1109/JESTPE.2021.3065671, IEEE Journal of Emerging and Selected Topics in Power Electronics

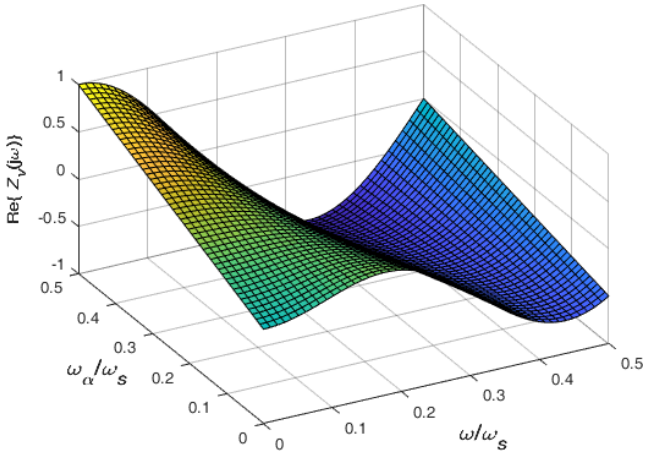

Fig. 5. The variations of the real part of $Z_v(j\omega)$ versus ω_α and ω.

The virtual impedance in the new control system can be expressed as

$$Z_v(s) = k_{pi} G_{bp}(s) e^{-1.5 T_s s} . \quad (6)$$

Achieving $Z_v(s)$ is similar to Fig. 2(b), and its related figure is not depicted again. From (6), it is noted that the negative effect of delay could be amended by $G_{bp}(s)$. If the lead-lag filter introduces an adequate positive phase, the virtual impedance will keep its positive real value over a wider frequency range and, therefore, the critical frequency will be expanded.

B. Tuning Lead-Lag Filter Parameters

Using (6), the real part of virtual impedance in the frequency domain could be represented as follows:

$$Re\{Z_v(j\omega)\} = \frac{k_{pi}k_{bp}}{\omega^2+\omega_\beta^2}[(\omega_\alpha\omega_\beta+\omega^2)\cos(1.5\omega T_s)+\omega(\omega_\beta-\omega_\alpha)\sin(1.5\omega T_s)] . \quad (7)$$

It is clear that the current controller gain (k_{pi}) and lead-lag filter gain (k_{bp}) have no effect on the phase of virtual impedance and only affect the magnitude of $Z_v(s)$. Therefore, they must be tuned so that the resonance peak is mitigated and an adequate bandwidth for the control system is achieved.

To avoid the noise amplification, ω_β should be designed so that the magnitude of $G_{bp}(s)$ is preserved in a reasonable range at high frequencies. To this end, the Nyquist frequency can be considered as an upper limit, since Nyquist frequency should not exceed because of sampling effects found in a digitally-controlled system. Therefore, ω_β is selected as $0.5\omega_s$, where $\omega_s = 2\pi f_s$, and f_s is the sampling frequency.

Regarding the cutoff frequency ω_α, a graphical design approach is used for tuning. Fig. 5 shows the variations of the real part of $Z_v(j\omega)$ versus ω and ω_α. The per-unit values of ω and ω_α are used in this figure, for the sake of clearness. The system parameters summarized in Table I show that the resonance frequency of the filter capacitor and inverter-side inductor is 1768 Hz. Therefore, ω_α should be selected so that the real value of $Z_v(j\omega)$ remains positive at a rather wide neighborhood of this frequency to ensure that parameter tolerance in real applications does not affect the stability.

TABLE I
Parameters of the inverter and grid

Parameters of inverter	
Input DC voltage, V_{dc}	650 V
Inverter-side inductor, L_1	1.8 mH
Filter capacitor, C	4.5 μF
Grid-side inductor, L_2	0.5 mH
Resonance frequency, f_r	1768 Hz
Sampling and switching frequency, f_s	10 kHz
Rated power of each inverter	2.2 kVA
Parameters of utility grid	
Grid Voltage, V_g	400 V (Line to line)
Frequency	50 Hz
Grid inductance, L_g	$0 < L_g < 2.5$ mH

From Fig. 5, it is observed that $\omega_\alpha = 0.1\omega_s$ is a wise choice, as it makes the real value of $Z_v(j\omega)$ positive for the frequencies up to 2400 Hz. It means that the critical frequency expands from $f_s/6$ to 2400 Hz. As can be seen in Fig. 5, the maximum frequency that the lead-lag filter keeps the real part of $Z_v(j\omega)$ positive is about 2800 Hz, which is achieved by selecting $\omega_\alpha = 0$. After tuning ω_α and ω_β, the gain of lead-lag filter (k_{bp}) should be designed. Regarding (6), k_{bp} only affects the magnitude of $Z_v(s)$ and it is selected as $k_{bp} = 20$, in this paper.

C. Design of Voltage and Current Controllers

For the outer voltage control, an integral-resonant (IR) controller in the $\alpha\beta$ frame is used instead of the conventional PR controller. The IR controller could be presented in the s-domain as follows.

$$G_v(s) = \frac{k_{pv}}{s} + k_{rv}\frac{s}{s^2+2\omega_c s+\omega_o^2} \quad (8)$$

The first term in the right-side of (8), i.e., k_{pv}/s is the integral part of the controller, while the second term is the resonant part of the controller that is used for eliminating the steady-state error at the fundamental frequency.

The integral part of the IR controller increases the loop gain of the control system at lower frequencies and therefore, it helps the system to have a wide control bandwidth [38]. The resonant part of the IR controller at the fundamental frequency should be high enough to minimize the steady-state error. Therefore, $k_{rv} = 500$ is selected.

To tune the integral gain of the IR controller (k_{pv}) and the inner loop proportional (k_{pi}) so that the stability is guaranteed, the discretized form of the system loop gain (T) is derived by applying the ZOH transformation to the plant as follows:

$$T(z) = \frac{G_v(z)k_{pi}(1-\cos(\omega_r T_s))(z+1)}{z(z^2-2z\cos(\omega_r T_s)+1)+C\omega_r k_{pi}\sin(\omega_r T_s)(z-1)G_{bp}(z)} \quad (9)$$

where, ω_r is equal to $1/\sqrt{L_1 C}$. It should be noted that the voltage controller, $G_v(z)$ as well as lead-lag controller $G_{bp}(z)$ in (9) are discretized using Tustin method. The procedure of deriving (9) is completely explained in [25] and [39]. Therefore, it is not repeated here to save space.

This article has been accepted for publication in a future issue of this journal, but has not been fully edited. Content may change prior to final publication. Citation information: DOI 10.1109/JESTPE.2021.3065671, IEEE Journal of Emerging and Selected Topics in Power Electronics

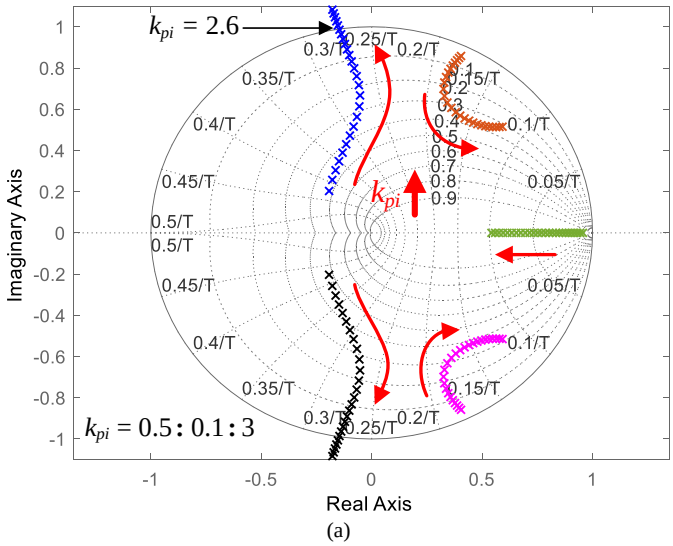

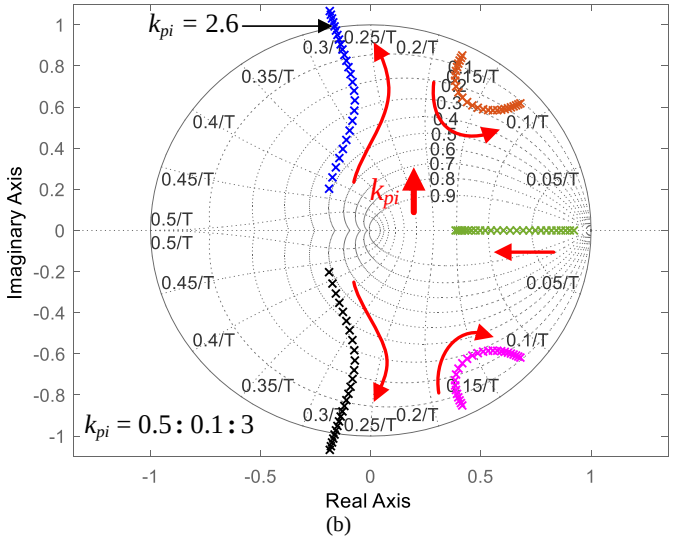

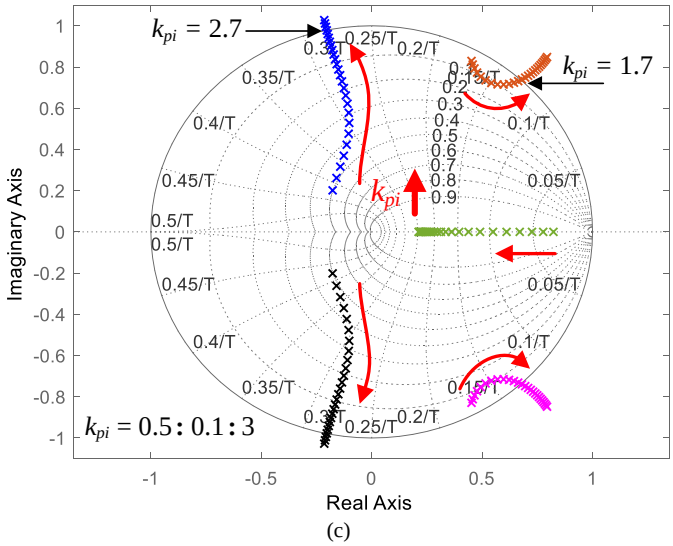

Fig. 6. The closed-loop poles movement of the control system. (a) k_{pv} = 500. (b) k_{pv} = 1000. (c) k_{pv} = 1500.

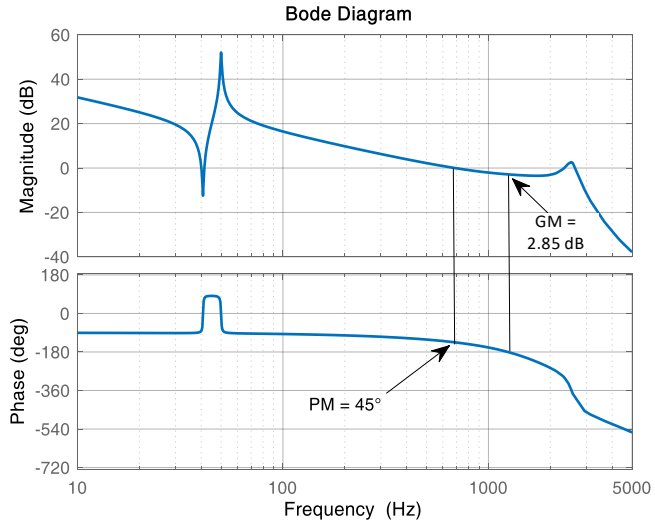

Fig. 7. The Bode diagram of the loop gain of the control system.

Fig. 6 shows the closed-loop pole maps with three typical k_{pv} values. A sweep of k_{pi} from 0.5 to 3 is performed at the step of 0.1 to identify the range of control parameters. As shown in Fig. 6(a), the poles with k_{pv} = 500 move outside the unit circle for $k_{pi} \geq 2.6$. The condition is the same for Fig. 6(b) for k_{pv} = 1000. However, in the case of k_{pv} = 1500, the closed-loop poles move outside the unit circle for $k_{pi} \geq 1.7$.

Through plotting the Bode diagram, it could be found that selecting k_{pv} = 1000 and k_{pi} = 2.5 gives the widest bandwidth in comparison with other values for k_{pv} and k_{pi}. Fig. 7 shows the Bode plot of $T(z)$ using the parameters presented in Table II, when delay compensation is applied. It could be seen that the control system has an acceptable bandwidth thanks to the IR controller which mitigates the low order harmonics and meets the control requirements.

IV. Passivity Enhancement Using Output Current Feedforward Method

The Thevenin equivalent circuit of a voltage-controlled inverter could be achieved from Fig. 4 as shown in Fig. 8, where $Z_o(s)$ is the inverter output impedance and $G_{cl}(s)$ is the transfer function of the closed-loop control system, i.e., $G_{cl}(s) = T(s) / [T(s) + 1]$. The inverter output impedance $Z_o(s)$ could be derived from Fig. 4, as follows:

$$Z_o(s) = \left.\frac{v_o(s)}{-i_o(s)}\right|_{Vref=0}$$

$$= \frac{Z_{L1}Z_C + k_{pi}G_d(s)G_{bp}(s)Z_C}{Z_{L1} + Z_C + k_{pi}G_d(s)G_{bp}(s) + G_v(s)k_{pi}G_d(s)Z_C}$$

$$= \frac{sL_1 + k_{pi}G_d(s)G_{bp}(s)}{s^2L_1C + 1 + sCk_{pi}G_d(s)G_{bp}(s) + G_v(s)k_{pi}G_d(s)}. \quad (10)$$

Based on the passivity-based stability criterion, satisfying two following constraints is necessary for a voltage-controlled

This article has been accepted for publication in a future issue of this journal, but has not been fully edited. Content may change prior to final publication. Citation information: DOI 10.1109/JESTPE.2021.3065671, IEEE Journal of Emerging and Selected Topics in Power Electronics

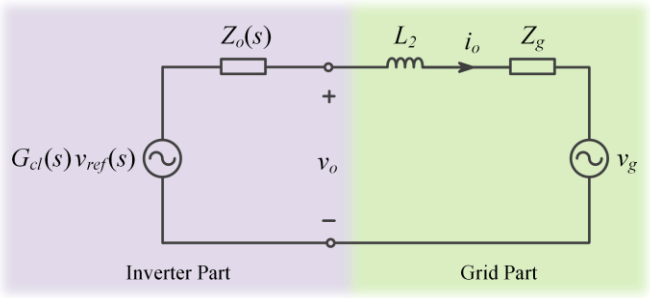

Fig. 8. The Thevenin equivalent circuit of a voltage-controlled inverter.

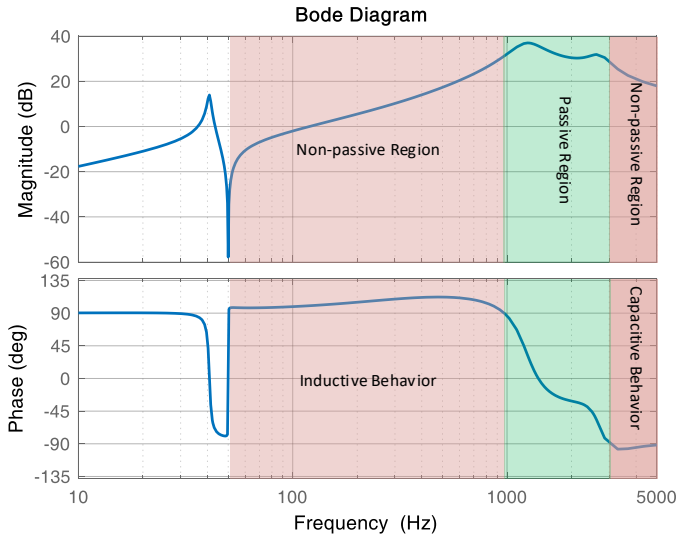

Fig. 9. The Bode diagram of $Z_o(s)$ without the output current feedforward loop.

inverter to keep its stability [31]. 1) It should have no RHP poles in its closed-loop transfer function, which means that the inverter should be internally stable. 2) The real part of the inverter output impedance must be positive, which implies that the phase of inverter output impedance must be in the interval of [−90°, 90°] at all frequencies.

The dual-loop control system can shrink those frequencies that inverter is non-passive by its inherent active damping. However, a region around the resonance frequency might still remain that the phase of $Z_o(s)$ exceeds ±90°. If the grid impedance and $Z_o(s)$ intersect in this area, it may put the system at the risk of instability. Such a scenario can happen in weak grids, where the grid impedance varies widely or in multi-parallel systems, where the coupling effect among inverters changes the grid impedance seen by each inverter. Therefore, the passivity-based stability is applied in this paper to mitigate the non-passive parts of $Z_o(s)$ and to provide a condition that the inverter can work stably irrespective of non-ideal grid conditions.

As depicted in Fig. 7, the inverter can work stably in a stiff grid since the control system satisfies the phase margin and gain margin constraints. Therefore, the first constraint is satisfied. However, the effects of grid impedance and grid-side inductor are not considered in this Bode plot. Therefore, the system might become unstable in non-stiff grids. The inverter

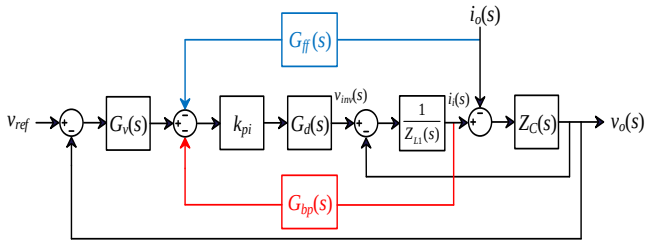

Fig. 10. The control scheme of the proposed strategy consists of delay compensation and output current feedforward.

output impedance could be analyzed for stability assessment in a non-stiff grid.

The Bode plot of $Z_o(s)$ up to the Nyquist frequency is depicted in Fig. 9. This figure shows that there is a wide range that the phase of $Z_o(s)$ exceeds ±90°. In most of this non-passive area, $Z_o(s)$ has an inductive behavior that does not put the system at the risk of instability in distribution grids, which the grid impedance is mostly inductive or resistive-inductive. However, the capacitive behavior of $Z_o(s)$ in high frequencies might make the system unstable when it interacts with an inductive grid impedance. To ensure about the stable operation of two paralleled subsystems, the output impedance of those subsystems must have a positive phase margin where their Bode plots intersect at the frequency f_i, i.e.

$$\mathrm{PM} = 180° - [\angle Z_g(f_i) - \angle Z_o(f_i)]\,. \tag{11}$$

An output current feedforward method as shown in Fig. 10 is proposed in this paper to make the inverter totally passive. According to this structure, the inverter output impedance using the proposed method could be achieved as

$$\begin{aligned} Z_o(s) &= \frac{Z_{L1}Z_C + k_{pi}G_d(s)G_{bp}(s)Z_C + k_{pi}G_{ff}(s)G_d(s)Z_C}{Z_{L1} + Z_C + k_{pi}G_d(s)G_{bp}(s) + G_v(s)k_{pi}G_d(s)Z_C} \\ &= \frac{sL_1 + k_{pi}G_d(s)G_{bp}(s) + k_{pi}G_{ff}(s)G_d(s)}{s^2L_1C + 1 + sCk_{pi}G_d(s)G_{bp}(s) + G_v(s)k_{pi}G_d(s)}\,. \end{aligned} \tag{12}$$

Notice that this feedforward loop does not affect the closed-loop transfer function $G_{cl}(s)$ defined in (10) and only changes the inverter output impedance. Notice that the feedforward transfer function $G_{ff}(s)$ only appears in the numerator of (12). Therefore, the phase of $Z_o(s)$ can be boosted in the concerned frequency range by selecting $G_{ff}(s)$ as a lead-lag filter, as expressed below:

$$G_{ff}(s) = k_{ff}\frac{s+\omega_z}{s+\omega_p}\,. \tag{13}$$

In (13), k_{ff}, ω_z and ω_p are the gain and cutoff frequency of numerator and denominator, respectively. Regarding Fig. 9, the concerned frequency range, where the phase of $Z_o(s)$ needs to be increased, is higher than 3000 Hz. Hence, ω_z is selected as $2\pi\times3000$ rad/s. Also, ω_p is selected as $0.5\omega_s$ in order to prevent the noise amplification around the Nyquist frequency. Regarding (12), the phase of $Z_o(s)$ is related to various parameters that make it difficult to design k_{ff} to realize impedance passivity. Therefore, an intuitive graphical method is used to design the gain of the lead-lag filter (k_{ff}). Fig. 11 shows the phase of $Z_o(s)$ versus frequency and k_{ff}. As shown in

This article has been accepted for publication in a future issue of this journal, but has not been fully edited. Content may change prior to final publication. Citation information: DOI 10.1109/JESTPE.2021.3065671, IEEE Journal of Emerging and Selected Topics in Power Electronics

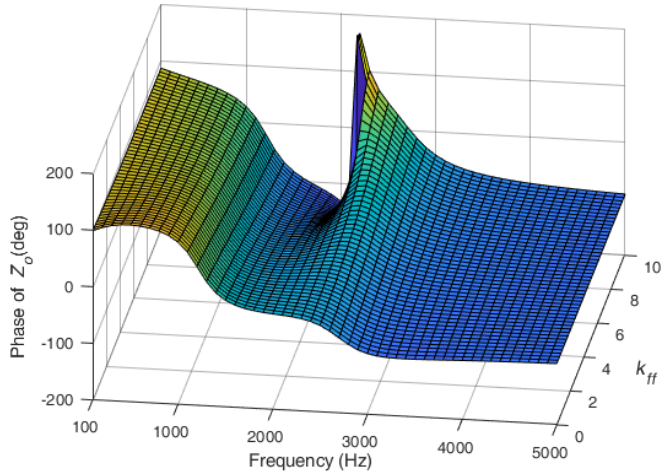

Fig. 11. The phase of $Z_o(s)$ versus frequency and k_{ff}.

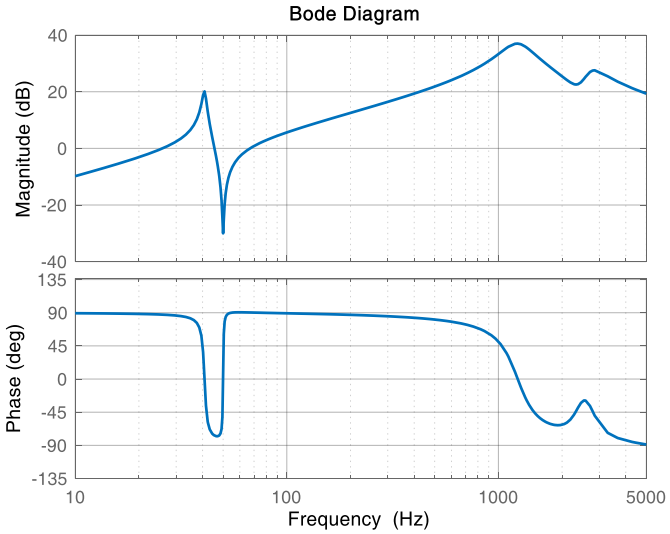

Fig. 12. The Bode diagram of $Z_o(s)$ with the proposed output current feedforward method.

this figure, when k_{ff} is higher than 8, $Z_o(s)$ has a non-passive behavior around 2000 Hz. On the other hand, for lower values of k_{ff}, the phase of $Z_o(s)$ exceeds −90° in higher frequencies. Therefore, k_{ff} = 5 is selected which is a tradeoff for the phase of $Z_o(s)$ in medium and high frequencies.

Fig. 12 presents the Bode diagram of $Z_o(s)$ with the proposed output current feedforward method. As shown in this figure, the non-passive region with capacitive behavior in high frequencies as well as the non-passive region with inductive behavior in medium frequencies is mitigated thanks to the feedforward loop. In this way, the passivity of the inverter is expanded till $f_s/2$. The passivity of inverter output impedance guarantees the stability of the system irrespective of grid impedance variations and the number of parallel inverters in a microgrid.

V. Experimental Results

Fig. 13 shows an experimental setup that is built up to validate the proposed output current feedforward and delay compensation method. Two-level three-phase *Danfoss*

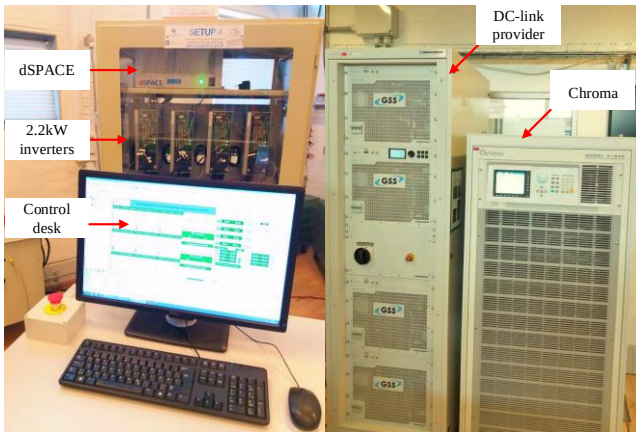

Fig. 13. The laboratory setup.

TABLE II
Control Parameters

Voltage controller	
k_{pv}	1000
k_{rv}	500
Current controller	
k_{pi}	2.5
Delay compensation controller $G_{bp}(s)$	
k_{bp}	20
ω_α	$0.1\omega_s$
ω_β	$0.5\omega_s$
Output current feedforward controller $G_{ff}(s)$	
k_{ff}	5
ω_z	$0.3\omega_s$
ω_p	$0.5\omega_s$

inverters with the rating power of 2.2 kW are used. The *dSPACE* DS1006 is used for the implementation of the control system. Also, a grid-simulator *Chroma 61845* is used as an ideal grid. The physical system parameters and control ones are summarized in Table I and Table II, respectively.

A. Effectiveness of the Expanding f_{cr}

To verify the effectiveness of expanding the critical frequency using the proposed method, the Bode plots of the control system loop gain with and without delay compensation method are depicted in Fig. 14. It could be observed in this figure, without using the delay compensation, the system has a non-minimum phase behavior and it is unstable. In fact, in this condition, the resonance frequency of the filter capacitor and inverter-side inductor is higher than $f_s/6$ (f_r = 1768 Hz) and the real part of virtual impedance becomes negative at the resonance frequency, which in turn, introduces RHP poles. However, by using the $G_{bp}(s)$ controller along the inner feedback path, the system can work stably since f_{cr} is expanded as elaborated in Section III-B.

Experiments are carried out with and without the delay compensation method, to validate the above analysis. In this experiment, the inverter is disconnected from the grid which means the inverter output current is equal to zero. At first, the control system employs the delay compensation method and

This article has been accepted for publication in a future issue of this journal, but has not been fully edited. Content may change prior to final publication. Citation information: DOI 10.1109/JESTPE.2021.3065671, IEEE Journal of Emerging and Selected Topics in Power Electronics

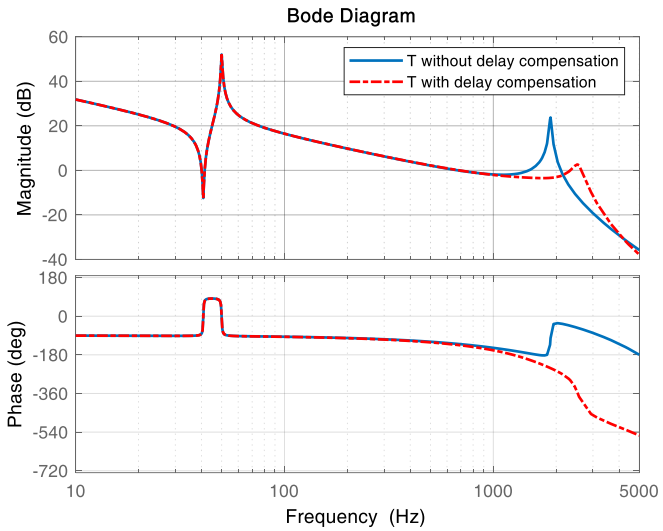

Fig. 14. The Bode diagram of the loop gain of the control system with and without delay compensation method.

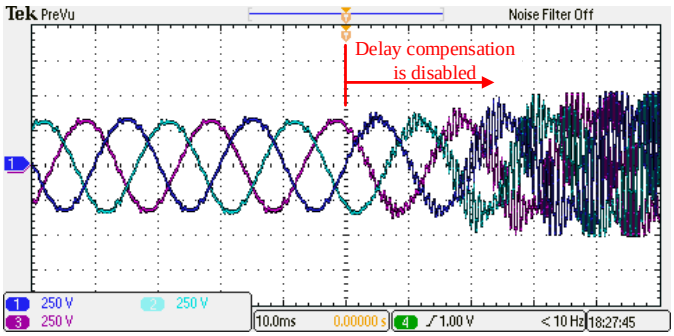

Fig. 15. The filter capacitor voltage in open-circuit condition with and without using the delay compensation method.

then, it is disabled to show the consequence of using the traditional dual-loop control method. Fig. 15 shows the filter capacitor voltage and it could be seen that the system works stably by using the delay compensation method. However, it becomes unstable when the delay compensation is disabled. It shows that the control system cannot work stably even in the open-circuit condition when the traditional dual-loop system is used and the resonance frequency is higher than $f_s/6$. The experimental results are compatible with the presented analysis and show the effectiveness of the controller design for widening the active damping area.

B. Stability Enhancement Using Output Current Feedforward Method

As presented in Figs. 7 and 9, although the system is stable in an ideal grid condition, there are non-passive areas in the frequency response of $Z_o(s)$, which might make the inverter unstable in weak grids. For the investigation of the stability of voltage-controlled inverters, grid-side inductor (L_2) could be considered as a part of the grid impedance and their lumped value ($L_t = L_2 + L_g$) could be evaluated for the impedance-based stability criterion. The Bode diagrams of the inverter output impedance, lumped grid impedance for L_g= 0.5 mH (L_t = 1 mH), and L_g = 2.5 mH (L_t = 3 mH) discarding the

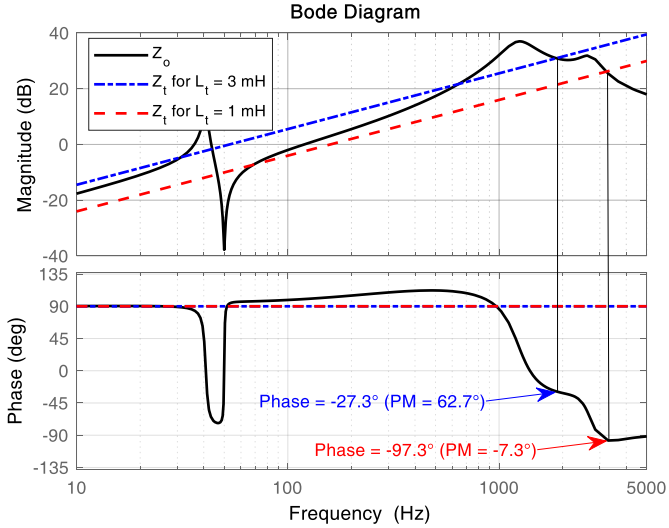

Fig. 16. The Bode diagrams of Z_o and Z_t without the proposed output current feedforward method.

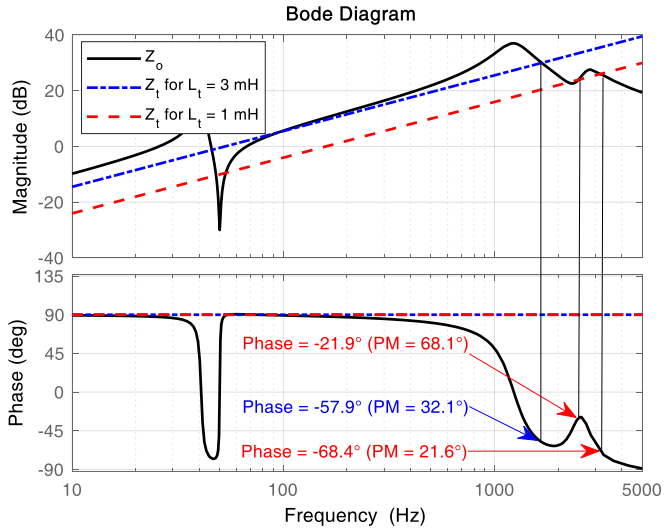

Fig. 17. The Bode diagrams of Z_o and Z_t with the proposed output current feedforward method.

output current feedforward loop is depicted in Fig. 16. As this figure shows, when L_g = 2.5 mH, the grid impedance and inverter output impedance intersect in the passive region with PM = 62.7° (according to (11)), which shows that the grid-connected inverter can work stably. However, when the grid inductance reduces to 0.5 mH (L_t = 1 mH), $Z_o(s)$ intersects with the corresponding impedance of L_t, i.e., $Z_t(s)$, in the forbidden area with PM = -7.3°, which shows the system loses its stability in this situation.

To cope with this problem, the output current feedforward method could be used. Fig. 17 shows the Bode diagram of the $Z_o(s)$ using the proposed method. As this figure shows, despite the previous case, the inverter keeps its stability irrespective of grid impedance variations since the phase of $Z_o(s)$ remains within [−90°, 90°] and hence, the inverter has a positive PM where $Z_o(s)$ and $Z_t(s)$ intersects.

This article has been accepted for publication in a future issue of this journal, but has not been fully edited. Content may change prior to final publication. Citation information: DOI 10.1109/JESTPE.2021.3065671, IEEE Journal of Emerging and Selected Topics in Power Electronics

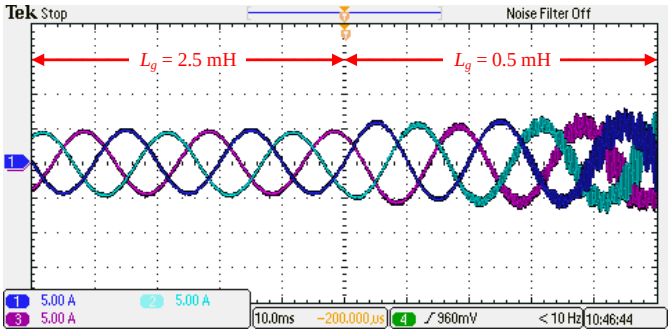

Fig. 18. Three-phase injected current to the grid without the output current feedforward method in the case of grid inductance variation.

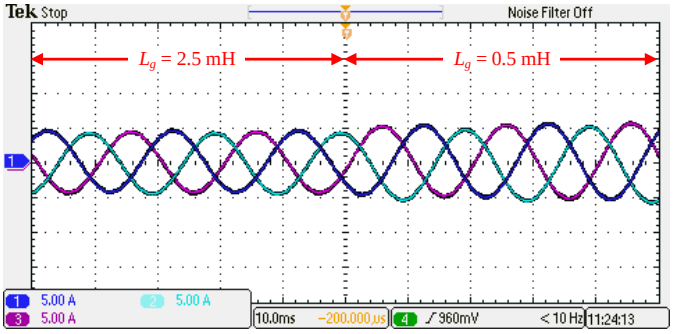

Fig. 19. Three-phase injected current to the grid using the output current feedforward method in the case of grid inductance variation.

To show the validity of the above analysis and capability of the proposed method, new experiments are examined with/without the output current feedforward technique. Fig. 18 shows the grid injected current while the output current loop is disabled and when the grid inductance changes from 2.5 mH to 0.5 mH. It could be seen that the current is stable with L_g = 2.5 mH. However, it becomes unstable when L_g decreases. The experimental validation of the proposed output current feedforward method is depicted in Fig. 19. As it is shown, the inverter remains stable irrespective of the grid impedance variations by using the proposed method. The experimental results in this section verify the analytical results associated with Figs. 16 and 17.

C. Stability Investigation Against the Parallel Inverters

In a microgrid that a lot of inverters are connected in parallel, the equivalent grid impedance that is seen by each inverter becomes different from the actual grid impedance due to the coupling effect of other inverters. Therefore, in addition to the grid impedance, the number of paralleled inverters can put the whole of the system at the risk of instability. To show the effectiveness of the proposed methods where a number of inverters are connected in parallel, the interconnection of two inverters as shown in Fig. 20 is investigated. The physical and control parameters of both inverters are similar and are presented in Table I and Table II, respectively. Also, L_g = 1 mH is selected for this study. By substituting the Thevenin equivalent circuit for each inverter presented in Fig. 20, the equivalent model of paralleled inverters can be obtained as shown in Fig. 21. It is worth mentioning that the equivalent Thevenin voltage source of inverters as well as grid voltage

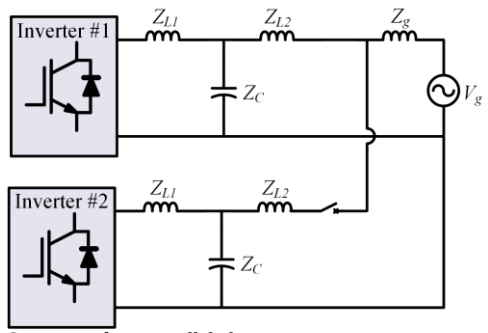

Fig. 20. Structure of two paralleled inverters.

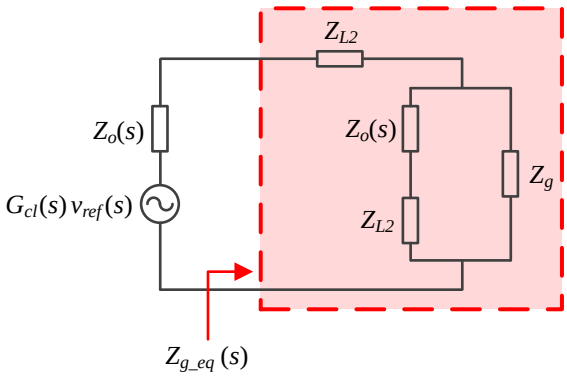

Fig. 21. The equivalent impedance schematic model for two paralleled inverters.

are supposed to be zero (short circuit) since they do not affect the equivalent grid impedance seen by inverters. As it could be seen in Fig. 21, the equivalent grid impedance (Z_{g_eq}) that is seen by each inverter, includes grid-side filter inductor, the grid impedance, and the inverter output impedance of the other paralleled inverter, as well. $Z_{g\_eq}(s)$ could be derived from Fig. 21 as

$$Z_{g\_eq}(s) = Z_g \,\|\, [Z_o(s) + Z_{L2}] + Z_{L2} \tag{14}$$

where the parallel connection of impedances is indicated by '||' sign. Therefore, for investigation of stability in a multi-paralleled system, Z_{g_eq} should be investigated instead of Z_g. Fig. 22 shows the Bode plots of $Z_o(s)$ without the output current feedforward, equivalent grid impedance Z_{g_eq} and also, grid impedance corresponding to a case in which only one inverter is connected to the grid (inverter sees $L_t = L_2 + L_g$ = 1.5 mH as grid impedance). As shown in Fig. 22, the system has a positive PM (PM = 4.9°) where $Z_o(s)$ and $Z_t(s)$ intersect, which means that a single inverter could be connected to the grid stably. However, when both inverters are connected, the system has a negative phase margin (PM = -143.1°) at the intersection point of $Z_o(s)$ and $Z_{g\_eq}(s)$. It implies that the parallel connection of two inverters is unstable.

To validate the capability of the proposed method, an investigation is done by using the output current feedforward method in Fig 23. As this figure shows, the inverter output impedance has a passive behavior and the PM is positive at the intersection points either in the case of a single or two paralleled inverters.

This article has been accepted for publication in a future issue of this journal, but has not been fully edited. Content may change prior to final publication. Citation information: DOI 10.1109/JESTPE.2021.3065671, IEEE Journal of Emerging and Selected Topics in Power Electronics

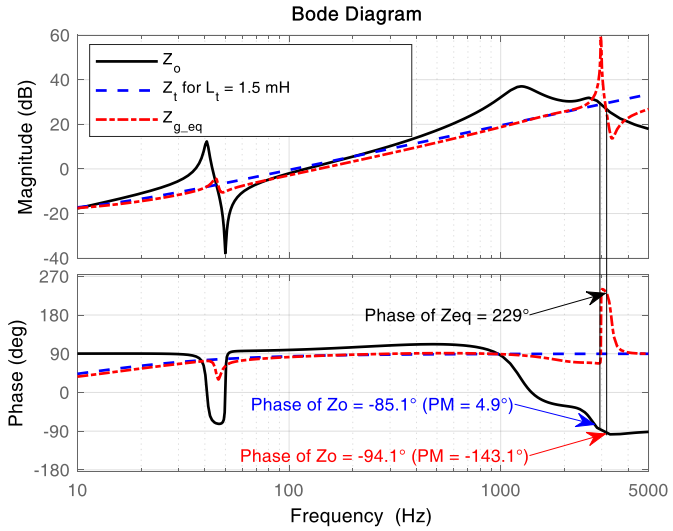

Fig. 22. The Bode diagrams of Z_o, Z_t, and Z_{g_eq} without the output current feedforward loop.

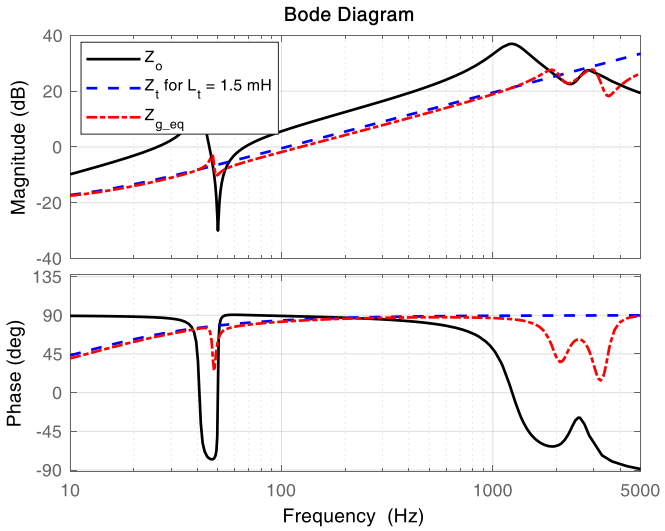

Fig. 23. The Bode diagrams of Z_o, Z_t, and Z_{g_eq} with the output current feedforward loop.

To investigate the above analysis, the experiment is done without the output current feedforward loop and the total grid injected current is shown in Fig. 24. In this experiment, the first inverter is supplying the grid and the second inverter is suddenly connected. As shown in this figure, inverter 1 is stable when it is connected to the grid individually. However, after the connection of the second inverter, both inverters become unstable because the equivalent grid inductance is changed and inverter output impedance has a non-passive behavior in the new intersection point.

The experiment is done once again with the proposed output current feedforward method. The experimental results are depicted in Fig. 25. It is clear that the system keeps its stability even after the connection of the second inverter, thanks to the passivity-based controller design that keeps the phase of the inverter output impedance within the passive area. The experimental results verify the conclusions drawn from Figs. 22 and 23.

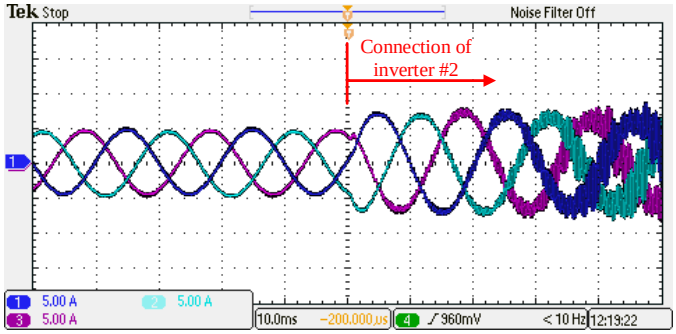

Fig. 24. The total injected current to the grid without the output current feedforward method.

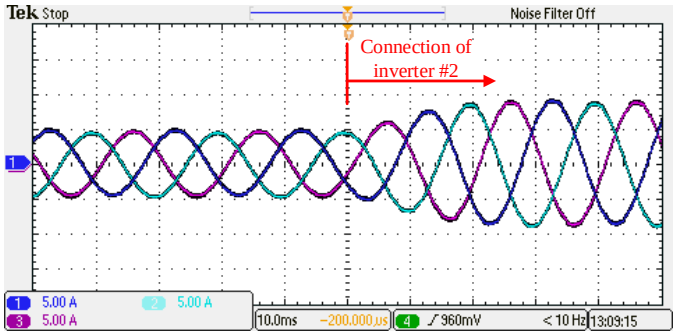

Fig. 25. The total injected current to the grid with the output current feedforward method.

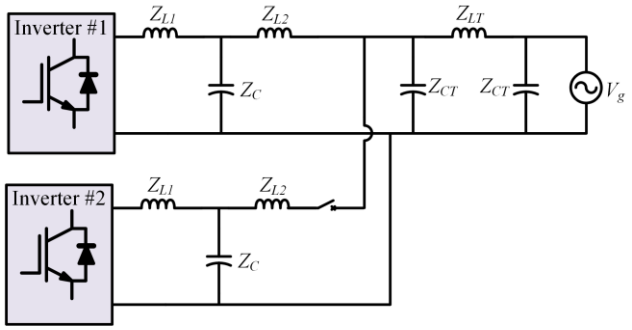

Fig. 26. Two paralleled grid-connected inverters with π-model grid

For the sake of generality, the model of grid impedance is substituted by a π-model as shown in Fig. 26. In this figure, Z_{LT} and Z_{CT} are the impedances associated with the inductance and capacitance of π-model, where L_T = 0.9 mH and C_T = 4.5 μF are considered. Fig. 27 shows the Bode diagram of inverter output impedance without using the output current feedforward method and equivalent grid impedance Z_{g_eq}. As can be seen in this figure, the system is unstable because it has a negative PM (PM = -175.6°) at the intersection point of $Z_o(s)$ and $Z_{g\_eq}(s)$. However, by using the proposed output current feedforward method, the phase of $Z_o(s)$ and $Z_{g\_eq}(s)$ are always within the passive area as Fig. 28 shows and consequently, the stability of the system is guaranteed.

The experiment is carried out to verify the above analysis. For this experiment, the output current feedforward is enabled at first, and then it becomes disable. Fig. 29 shows the total grid injected current. As shown in this figure, the system works well when the feedforward method is employed.

This article has been accepted for publication in a future issue of this journal, but has not been fully edited. Content may change prior to final publication. Citation information: DOI 10.1109/JESTPE.2021.3065671, IEEE Journal of Emerging and Selected Topics in Power Electronics

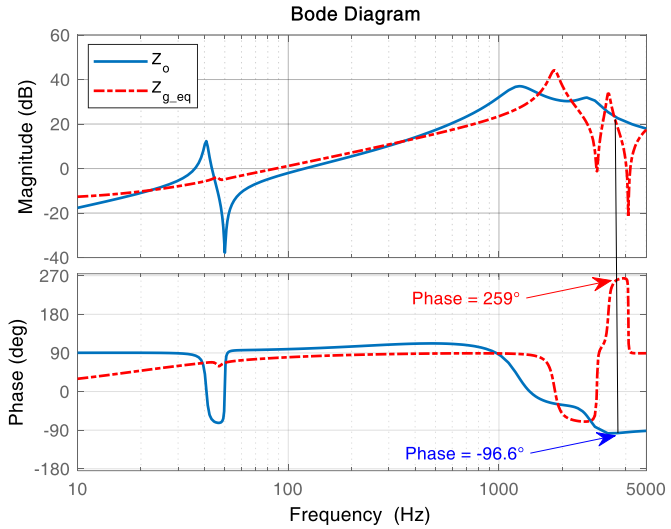

Fig. 27. The Bode diagrams of Z_o and Z_{g_eq} without the output current feedforward loop.

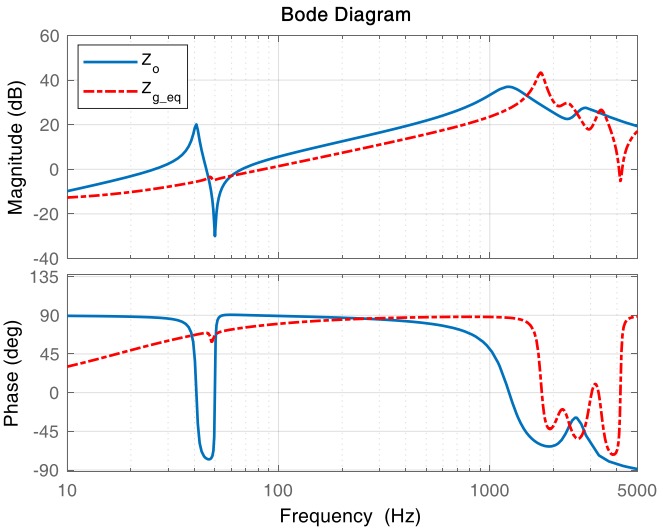

Fig. 28. The Bode diagrams of Z_o and Z_{g_eq} with the output current feedforward loop.

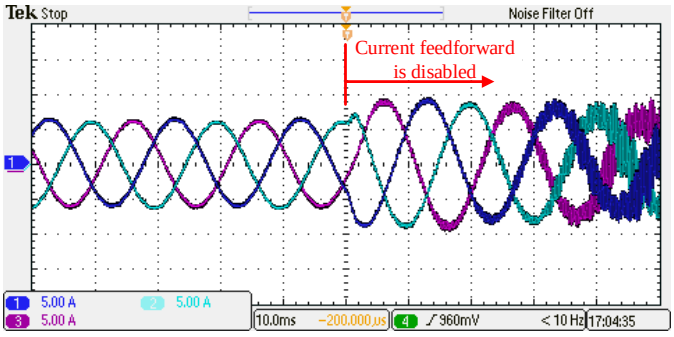

Fig. 29. The total injected current to the grid with π-model grid impedance.

However, the system goes toward instability after disabling the feedforward method.

The experimental results validate the capability and performance of the proposed methods and show that by expanding the critical frequency and improving the passivity of inverter output impedance, the inverter can work stably irrespective of grid impedance variations and coupling effect of parallel inverters. It is worthy to note that since the system has bounded-input bounded-output (BIBO) stability, changing the reference voltage as an input does not make the system unstable.

VI. Conclusion

A modified control system for stability enhancement of dual-loop voltage-controlled grid-connected in weak grids is presented in this paper. At first, it was shown that in traditional control systems, the delay causes an unintentionally negative virtual resistance, which introduces RHP poles when the resonance occurs in a frequency that is higher than $f_s/6$. To cope with this challenge, a lead-lag filter is inserted along the active damping loop to expand the critical frequency. In this way, it does not need extra sensors. Then, a feedforward method using the output current is employed that mitigates the non-passive region and keeps the phase of the inverter output impedance within [−90°, 90°] up to Nyquist frequency. In this way, the stable operation of grid-connected inverters is guaranteed irrespective of grid impedance variations and the coupling effect of parallel inverters in microgrids. The effectiveness of the control system is validated using analysis and experimental results in different case studies.

References

[1] Y. Han, M. Yang, H. Li, P. Yang, L. Xu, E. A. A. Coelho, and J. M. Guerrero "Modeling and stability analysis of *LCL*-type grid-connected inverters: A comprehensive overview," *IEEE Access*, vol. 7, pp. 114975-115001, 2019.

[2] Y. Deng, Y. Tao, G. Chen, G. Li, and X. He, "Enhanced power flow control for grid-connected droop-controlled inverters with improved stability," *IEEE Trans. Ind. Electron.*, vol. 64, no. 7, pp. 5919-5929, Jul. 2017.

[3] M. G. Judewicz, S. A. González, J. R. Fischer, J. F. Martnez, and D. O. Carrica, "Inverter-side current control of grid-connected voltage source inverters with *LCL* filter based on generalized predictive control," *IEEE J. Emerg. Sel. Topics Power Electron.*, vol. 6, no. 4, pp. 1732–1743, Dec. 2018.

[4] D. Pan, X. Ruan, X. Wang, H. Yu, and Z. Xing, "Analysis and design of current control schemes for *LCL*-type grid-connected inverter based on a general mathematical model," *IEEE Trans. Power Electron.*, vol. 32, no. 6, pp. 4395–4410, Jun. 2017.

[5] A. Akhavan, J. C. Vasquez, and J. M. Guerrero, "A simple method for passivity enhancement of current controlled grid-connected inverters," *IEEE Trans. Power Electron.*, vol. 35, no. 8, pp. 7735-7741, Aug. 2020.

[6] X. Ruan, X. Wang, D. Pan, D. Yang, W. I. Li, and C. Bao, "Resonance damping methods of *LCL* filter," in *Control Techniques for LCL-Type Grid-Connected Inverters*. Beijing, China: Springer, 2018, ch. 8, pp. 165–196.

[7] X. Wang, F. Blaabjerg, and P. C. Loh, "Grid-current-feedback active damping for *LCL* resonance in grid-connected voltage-source converters," *IEEE Trans. Power Electron.*, vol. 31, no. 1, pp. 213-223, Jan. 2016.

[8] D. Pan, X. Ruan, C. Bao, W. Li, and X. Wang, "Capacitor-current-feedback active damping with reduced computation delay for improving robustness of *LCL*-Type grid connected inverter," *IEEE Trans. Power Electron.*, vol. 29, no. 7, pp. 3414–3427, Jul. 2014.

[9] S. Y. Park, C. L. Chen, J. S. Lai, and S. R. Moon, "Admittance compensation in current loop control for a grid-tie *LCL* fuel cell inverter," *IEEE Trans. Power Electron.*, vol. 23, no. 4, pp. 1716–1723, Jul. 2008.

[10] Y. Jia, J. Zhao, and X. Fu, "Direct grid current control of *LCL*-filtered

grid-connected inverter mitigating grid voltage disturbance," *IEEE Trans. Power Electron.*, vol. 29, no. 3, pp. 1532–1541, Mar. 2014.

[11] J. Xu, S. Xie, and T. Tang, "Active damping-based control for grid-connected *LCL*-filtered inverter with injected grid current feedback only," *IEEE Trans. Ind. Electron.*, vol. 61, no. 9, pp. 4746–4758, Sep. 2014.

[12] Q. C. Zhong and T. Hornik, "Cascaded current-voltage control to improve the power quality for a grid-connected inverter with a local load," *IEEE Trans. Ind. Electron.*, vol. 60, no. 4, pp. 1344–1355, Apr. 2013.

[13] X. Li, P. Lin, Y. Tang, K. Wang, "Stability design of single-loop voltage control with enhanced dynamic for voltage-source converters with a low *LC*-resonant-frequency", *IEEE Trans. Power Electron.*, vol. 33, no. 11, pp. 9937-9951, 2018.

[14] X. Wang, F. Blaabjerg, and Z. Chen, "Autonomous control of inverter-interfaced distributed generation units for harmonic current filtering and resonance damping in an islanded microgrid," *IEEE Trans. Ind. Appl.*, vol. 50, no. 1, pp. 452–461, Jan./Feb. 2014.

[15] K. Sung-Hun, H. Dehbonei, and C. V. Nayar, "Application of voltage and current-controlled voltage source inverters for distributed generation systems," *IEEE Trans. Energy*, vol. 21, no. 3, pp. 782–792, Sep. 2006.

[16] N. R. Averous, M. Stieneker, and R. W. De Doncker, "Grid emulator requirements for a multi-megawatt wind turbine test-bench," in *Proc. IEEE 11th Int. Conf. Power Electron. Drive Syst.*, 2015, pp. 419–426.

[17] P. C. Loh and D. G. Holmes, "Analysis of multiloop control strategies for *LC*/*CL*/*LCL*-filtered voltage-source and current-source inverters," *IEEE Trans. Ind. Appl.*, vol. 41, no. 2, pp. 644–654, Mar./Apr. 2005.

[18] K. Sozański, *Digital Signal Processing in Power Electronics Control Circuits*. Springer-Verlag, London, 2013.

[19] Y. Lyu, H. Lin, and Y. Cui, "Stability analysis of digitally controlled *LCL*-type grid-connected inverter considering the delay effect," *IET Power Electron.*, vol. 8, no. 9, pp. 1651-1660, Aug. 2015.

[20] Z. Xin, X. Wang, P. C. Loh, and F. Blaabjerg, "Grid-current-feedback control for *LCL*-filtered grid converters with enhanced stability," *IEEE Trans. Power Electron.*, vol. 32, no. 4, pp. 3216-3228, Apr. 2017.

[21] X. Wang, F. Blaabjerg, and P. C. Loh, "Virtual *RC* damping of *LCL*-filtered voltage source converters with extended selective harmonic compensation," *IEEE Trans. Power Electron.*, vol. 30, no. 9, pp. 4726–4737, Sep. 2015.

[22] D. Pan, X. Ruan, C. Bao, W. Li, and X. Wang, "Capacitor-current-feedback active damping with reduced computation delay for improving robustness of *LCL*-type grid-connected inverter," *IEEE Trans. Power Electron.*, vol. 29, no. 7, pp. 3414–3427, Jul. 2014.

[23] X. Li, X. W. Y. Geng, X. Yuan, C. Xia, and X. Zhang, "Wide damping region for *LCL*-type grid-connected inverter with an improved capacitor current- feedback method," *IEEE Trans. Power Electron.*, vol. 30, no. 9, pp. 5247–5259, Sep. 2015.

[24] V. Miskovic, V. Blasko, T. Jahns, A. Smith, and C. Romenesko, "Observer based active damping of *LCL* resonance in grid connected voltage source converters" in *Proc. IEEE Energy Convers. Congr. Expo*., 2013, pp. 4850–4856.

[25] D. Pan, X. Ruan, C. Bao, W. Li, and X. Wang, "Optimized controller design for *LCL*-type grid-connected inverter to achieve high robustness against grid-impedance variation", *IEEE Trans. Ind. Electron.*, vol. 62, no. 3, pp. 1537-1547, Mar. 2015.

[26] J. Sun, "Impedance-based stability criterion for grid-connected inverters," *IEEE Trans. Power Electron.*, vol. 26, no. 11, pp. 3075-3078, Nov. 2011.

[27] J. L. Agorreta, M. Borrega, J. López, and L. Marroyo, "Modeling and control of *N*-paralleled grid-connected inverters with *LCL* filter coupled due to grid impedance in PV plants," *IEEE Trans. Power Electron.*, vol. 26, no. 3, pp. 770-785, Mar. 2011.

[28] A. Akhavan, H. R. Mohammadi, and J. M. Guerrero, "Modeling and design of a multivariable control system for multi-paralleled grid-connected inverters with *LCL* filter," *Int J Electric Power Energy Syst.*, vol. 94, pp. 354–362, Jan. 2018.

[29] C. Yoon, H. Bai, R. N. Beres, X. Wang, C. L. Bak, and F. Blaabjerg, "Harmonic stability assessment for multiparalleled, grid-connected inverters," *IEEE Trans. Power Electron.*, vol. 7, no. 4, pp. 1388-1397, Oct. 2016.

[30] L. Harnefors, X. Wang, A. Yepes, and F. Blaabjerg, "Passivity-based stability assessment of grid-connected VSCs—An overview," *IEEE J. Emerg. Sel. Topics Power Electron.*, vol. 4, no. 1, pp. 116–125, Mar. 2016.

[31] X. Wang, F. Blaabjerg, and P. C. Loh, "Passivity-based stability analysis and damping injection for multiparalleled VSCs with *LCL* filters," *IEEE Trans. Power Electron*, vol. 32, no. 11, pp. 8922-8935, Nov. 2017.

[32] X. Wang, P. C. Loh, and F. Blaabjerg, "Stability analysis and controller synthesis for single-loop voltage-controlled VSIs," *IEEE Trans. Power Electron*., vol. 32, no. 9, pp. 7394–7404, Sept. 2017.

[33] H. Bai, X. Wang, P. C. Loh, and F. Blaabjerg, "Passivity enhancement of grid-tied converters by series *LC*-filtered active damper," *IEEE Trans. Ind. Electron.*, vol. 64, no. 1, pp. 369-379, Jan. 2017.

[34] Y. He, H. S. Chung, C. Lai, X. Zhang, and W. Wu, "Active cancelation of equivalent grid impedance for improving stability and injected power quality of grid-connected inverter under variable grid condition," *IEEE Trans. Power Electron*., vol. 33, no. 11, pp. 9387-9398, Nov. 2018.

[35] L. Harnefors, A. G. Yepes, A. Vidal, and J. Doval-Gandoy, "Passivity-based controller design of grid-connected VSCs for prevention of electrical resonance instability," *IEEE Trans. Ind. Electron.*, vol. 62, no. 2, pp. 702-710, Feb. 2015.

[36] M. A. Abusara, S. M. Sharkh, and J. M. Guerrero, "Improved droop control strategy for grid-connected inverters," *Sustain. Energy, Grids Netw*., vol. 1, pp. 10–19, 2015.

[37] A. Akhavan, H. R. Mohammadi, J. C. Vasquez, and J. M. Guerrero, "Passivity-based design of plug-and-play current-controlled grid-connected inverters," *IEEE Trans. Power Electron*, vol. 35, no. 2, pp. 2135-2150, Feb. 2020.

[38] Y. Liao and X. Wang, "Evaluation of voltage regulators for dual-loop control of voltage-controlled VSCs," in Proc. *IEEE Energy Convers. Congr. Expo.*, 2019, pp. 5036-5042.

[39] S. Buso and P. Mattavelli, *Digital Control in Power Electronics*, San Rafael, CA, USA: Morgan & Claypool Publ., 2006.